Research article

Midya Parto, William E. Hayenga, Alireza Marandi, Demetrios N. Christodoulides
and Mercedeh Khajavikhan*

Nanolaser-based emulators of spin Hamiltonians

Abstract: Finding the solution to a large category of optimization problems, known as the NP-hard class, requires an exponentially increasing solution time using conventional computers. Lately, there has been intense efforts to develop alternative computational methods capable of addressing such tasks. In this regard, spin Hamiltonians, which originally arose in describing exchange interactions in magnetic materials, have recently been pursued as a powerful computational tool. Along these lines, it has been shown that solving NP-hard problems can be effectively mapped into finding the ground state of certain types of classical spin models. Here, we show that arrays of metallic nanolasers provide an ultra-compact, on-chip platform capable of implementing spin models, including the classical Ising and XY Hamiltonians. Various regimes of behavior including ferromagnetic, antiferromagnetic, as well as geometric frustration are observed in these structures. Our work paves the way towards nanoscale spin-emulators that enable efficient modeling of large-scale complex networks.

Keywords: nanolasers; nanophotonics; nonlinear optics; optical computing.

*Corresponding author: Mercedeh Khajavikhan, CREOL, The College of Optics and Photonics, University of Central Florida, Orlando, FL, USA; and Ming Hsieh Department of Electrical and Computer Engineering, University of Southern California, Los Angeles, CA, USA, E-mail: khajavik@usc.edu. https://orcid.org/0000-0002-7091-1470
Midya Parto and Demetrios N. Christodoulides: CREOL, The College of Optics and Photonics, University of Central Florida, Orlando, FL, USA. https://orcid.org/0000-0003-2100-5671 (M. Parto)
William E. Hayenga: Ming Hsieh Department of Electrical and Computer Engineering, University of Southern California, Los Angeles, CA, USA
Alireza Marandi: Department of Electrical Engineering, California Institute of Technology, Pasadena, CA, USA

1 Introduction

Enhancing the efficiency of various computational tasks has always been a major challenge in many and diverse fields. Over the years, this class of problems has been pursued in a number of fronts, like for example, in the classical works of Gauss and Lamé in number theory [1]. However, the field of computational complexity theory took a substantial leap in 1930s, after Turing proposed a general model for computing machines [2]. Using such standard models, it is believed that an important family of optimization problems – known as NP-hard – are challenging for conventional digital computers. Such optimization tasks are widely encountered in many important applications ranging from electronic chip testing and computer design to drug discovery and community detection [3–5]. Consequently, the past few years have witnessed intense research efforts in developing alternative computational platforms that may be capable of addressing such problems more efficiently than digital computers.

Lately, it has been shown that the solution of an NP-hard problem maps to finding the ground state of certain types of spin Hamiltonians with polynomial overhead [6–8]. Such spin Hamiltonians naturally arise in certain magnetic materials, representing the respective interactions among magnetic moments. In most cases, however, these magnetic materials lack the required versatility to be used for computational optimization. To address this issue, ultracold atoms in optical lattices have been employed to emulate magnetic spins [9–13] and most recently, active photonic platforms have been pursued as a viable means for experimental realization of spin Hamiltonians. In this regard, unlike passive implementations, such optical systems can identify the ground state of the corresponding Hamiltonian by their natural tendency to operate in the global minimum loss. Thus far, spin exchange interactions including classical Ising or XY Hamiltonians have been demonstrated in optical parametric oscillators (OPOs) [14–16], polaritonic simulators [17–19], degenerate laser cavities [20, 21], multicore fiber lasers [22], and spatial light modulators [23]. At this point, one may ask whether it is possible to exploit the vectorial degrees of freedom of light [24] in nanoscale structures in order to develop ultracompact photonic spin

simulators. If so, such on-chip nanophotonic arrangements could potentially enable large-scale optical emulators to address NP-hard optimization tasks in a scalable manner.

Quite recently, we reported [25] an experimental realization of spin Hamiltonians in arrays of active metallic nanocavities [26–30]. In this Letter, we discuss the details of the theoretical model that is responsible for such spin-like behavior in these arrangements. In particular, using a detailed electromagnetic (EM) analysis, it will be shown that the orientation of vectorial modal light fields in such nanocavities can naturally assume the role of an artificial "pseudospin". Analytical expressions obtained for the average EM loss in such nanolaser lattices suggest that these systems are formally isomorphic to different types of spin Hamiltonians. Moreover, we show that by properly designing the individual cavities to lase in pre-specified resonant modes, one would be able to implement the classical Ising Hamiltonian, in addition to the previously demonstrated XY Hamiltonian with both ferromagnetic (FM) and antiferromagnetic (AF) spin exchange couplings. In some scenarios involving XY Hamiltonians with AF couplings, our linear finite-element (FEM) simulations confirm geometrical frustration in the associated lasing supermodes, as expected from analytical results. Finally, we briefly discuss the outlook for exploiting our proposed platform in Hamiltonian optimization and computational applications.

2 Arrays of metallic nanolasers

To begin our analysis, let us consider an array of N identical metallic nanodisk lasers arranged in a circular fashion, as shown schematically in Figure 1 for $N = 5$. Here, the presence of the metallic cladding together with the overlapping near-fields of the adjacent cavities lead into a dissipative nearest-neighbor coupling. Under such conditions, one can obtain the EM fields associated with the resonant modes of each nanodisk from the longitudinal field components. For instance, for the transverse electric (TE) family of modes, the transverse distribution of the EM fields in nanodisk j is given by

$$
\begin{aligned}
E_{\rho,j} &\propto \frac{n}{\rho} J_n(k_\rho \rho) \sin(n\phi + \phi_j) \\
E_{\phi,j} &\propto [J_{n-1}(k_\rho \rho) - J_{n+1}(k_\rho \rho)] \cos(n\phi + \phi_j) \\
H_{\rho,j} &\propto -[J_{n-1}(k_\rho \rho) - J_{n+1}(k_\rho \rho)] \cos(n\phi + \phi_j) \\
H_{\phi,j} &\propto \frac{n}{\rho} J_n(k_\rho \rho) \sin(n\phi + \phi_j).
\end{aligned}
\tag{1}
$$

Similarly, the associated EM field components for the transverse magnetic (TM) family of modes can be found as

$$
\begin{aligned}
E_{\rho,j} &\propto [J_{n-1}(k_\rho \rho) - J_{n+1}(k_\rho \rho)] \cos(n\phi + \phi_j) \\
E_{\phi,j} &\propto -\frac{n}{\rho} J_n(k_\rho \rho) \sin(n\phi + \phi_j) \\
H_{\rho,j} &\propto \frac{n}{\rho} J_n(k_\rho \rho) \sin(n\phi + \phi_j) \\
H_{\phi,j} &\propto [J_{n-1}(k_\rho \rho) - J_{n+1}(k_\rho \rho)] \cos(n\phi + \phi_j).
\end{aligned}
\tag{2}
$$

In the above equations, n is the azimuthal mode number while ρ, ϕ represent the local coordinates in each nanodisk. It should be noted that in nanolasers, a small variation in the radii of the disks can result in the selection of a different mode. In our analysis, the field distributions have the same form in all the array elements, while their relative orientations can change from one nanocavity to another. Given the above field distributions, for TE group of modes, the total EM power dissipated in the metallic walls among the nanocavities can be obtained as [25]

$$
\begin{aligned}
\mathcal{P}_{L,TE} \propto \mathcal{P}_0^{TE} + (-1)^{n+1} \sum_{j=1}^{N} &\left\{ \mathcal{P}_{j,j+1}^{TE,1} \cos[\phi_{j+1} - \phi_j] \right. \\
&\left. + \mathcal{P}_{j,j+1}^{TE,2} \cos\left[\phi_{j+1} + \phi_j + 2j \times \frac{2n\pi}{N}\right] \right\}.
\end{aligned}
\tag{3}
$$

On the other hand, one can find the total EM loss associated with the TM modes to be

$$
\begin{aligned}
\mathcal{P}_{L,TM} \propto \mathcal{P}_0^{TM} + (-1)^{n} \sum_{j=1}^{N} \mathcal{P}_{j,j+1}^{TM} &\left\{ \cos[\phi_{j+1} - \phi_j] \right. \\
&\left. + \cos\left[\phi_{j+1} + \phi_j + 2j \times \frac{2n\pi}{N}\right] \right\}.
\end{aligned}
\tag{4}
$$

Equations (3) and (4) clearly show that the total dissipated power in the nanolaser array described here depends on the relative orientation of the vectorial EM modes in the individual cavity elements (ϕ_j). In other words, one can assign a pseudospin to the field distribution in each individual cavity as depicted in Figure 1. The overall loss endured by each collective supermode of the system is then effectively determined by the orientation of these pseudospins. In this regard, the above loss functions represent the spin Hamiltonians for the particular modes of interest with various azimuthal orders. Once gain exceeds the lasing threshold of the system, the resulting lasing supermode satisfies the minimum conditions for the loss functions described above. Therefore, Eqs. (3) and (4) play the role of an equivalent energy landscape function which is minimized by the structure when it starts to lase. This can be formally established by defining the following equivalent Hamiltonian
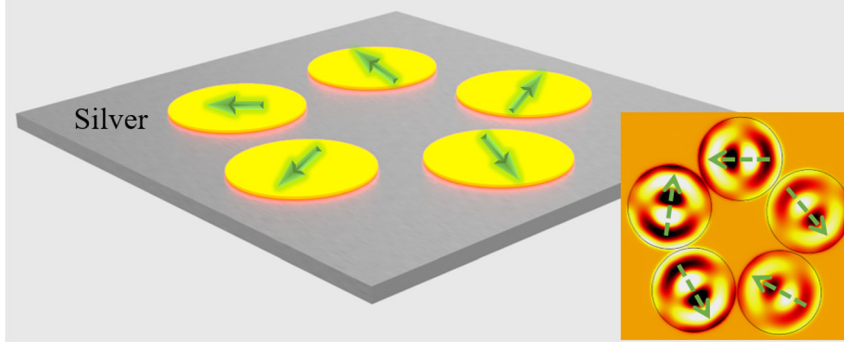
Figure 1: A schematic picture of an array of $N = 5$ metallic nanodisk lasers used in this study. The green arrows depict the orientation of the pseudospins. The inset shows lasing mode of a five-element nanodisk laser array as obtained from FEM simulations. The rotation of the local resonant modes is illustrated with dashed arrows, indicating the pseudospins.

associated with the *TE* and *TM* family of modes in the metallic nanolaser arrays considered here:

$$\mathcal{H} = \sum_{j=1}^{N} J_{j,j+1} \vec{\sigma}_j \cdot \vec{\sigma}_{j+1} + \sum_{j=1}^{N} J_{0j,j+1} \cos\left[\phi_j + \phi_{j+1} + 2j \times 2n\pi/N\right], \quad (5)$$

where $\vec{\sigma}_j$ is the classical pseudospin per each individual nanocavity defined as $\vec{\sigma}_j = (\cos\phi_j, \sin\phi_j)$. The exchange interaction coefficients $J_{i,j}$ and $J_{0i,j}$ are polarization mode dependent and can be tuned via the structure geometry (see Section 3). Depending on the azimuthal mode number n, the Hamiltonian of Eq. (5) can represent a number of different spin-exchange interactions which will be discussed in what follows.
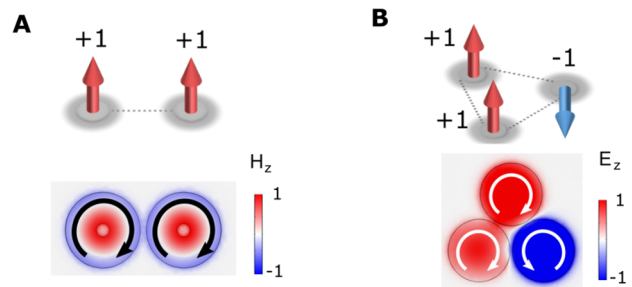
2.1 Realizing the classical Ising Hamiltonian

When the magnetic moments (spins) in a spin Hamiltonian are bound to vary in one spatial dimension (e.g., z-direction), the resulting Hamiltonian describes an Ising model. In our nanolaser platform, for TE_{0m} and TM_{0m} modes, the Hamiltonian $\mathcal{H}$ of Eq. (5) assumes the following simple form, representing a classical Ising Hamiltonian:

$$\mathcal{H}_{Ising} = \sum_{j=1}^{N} J_{j,j+1} s_j s_{j+1}, \quad (6)$$

where $s_j = \cos\phi_j$ play the role of one-dimensional Ising pseudospins, since in the weak coupling regime one can assume that $s_j \approx \pm 1$. Under these conditions, the resonant modes can be described by scalar variables, thereby implementing the Ising pseudospins with one-dimensional degrees of freedom. In addition, to achieve the aforementioned weak couplings, we place the nanocavities in close proximity in such a way that they are separated by a thin layer of metal. The associated exchange couplings $J_{i,j}$ can be tuned via the structure geometry and the type of the resonant mode within nanolasers (TE_{0m} or TM_{0m}). Figure 2

shows simulation results for different geometries in relation with the Hamiltonian of Eq. (6). To promote the TE_{0m} resonant modes in our system, we use metallic coaxial nanolasers, which feature a metallic cylindrical rod in the center of a nanodisk cavity [29]. As shown in Figure 2A, a TE_{01} lasing mode in coupled coaxial nanolasers separated by metallic cladding leads to a negative exchange coupling $J_{12} < 0$, as expected from an FM Ising Hamiltonian. Therefore, in order to minimize this Hamiltonian, such a system tends to lase in the in-phase supermode, akin to the ground state of the corresponding Ising Hamiltonian. On the other hand, by judiciously designing the size and geometry of the nanocavities in our proposed platform, one can obtain lasing in a TM_{01} resonant mode. This can be accomplished by matching the resonant frequency of the individual nanolasers with the gain bandwidth of the active material. Figure 2B presents a degenerate ground state of an Ising Hamiltonian with AF couplings in a triangle configuration, together with the simulated lasing supermode emerging in a three-element nanodisk laser array used to implement such a Hamiltonian.


Figure 2: Realizing the Ising Hamiltonian in nanolasers. (A) Ising spins with FM exchange interaction implemented by the TE_{01} modes in coaxial nanolasers. The black arrows show the direction of the azimuthal electric fields. (B) A three-element Ising Hamiltonian with AF couplings realized using a TM_{01} resonant mode of the nanodisk lasers. One of the possible degenerate ground states is presented here. The white arrows show the direction of the azimuthal magnetic fields within the resonators.

2.2 Higher-order lasing modes and the XY Hamiltonian

We next consider the case when the nanolaser elements are designed to predominantly lase in the higher-order modes with $n \neq 0$. Under such conditions, the pseudospins $\vec{\sigma}_j$ defined in Eq. (5) assume 2-dimensional degrees of freedom. In this scenario, the exchange terms in the first sum of Eq. (5) form the well-known XY Hamiltonian $\mathcal{H}_{XY}$. The total Hamiltonian can therefore be reformulated as $\mathcal{H} = \mathcal{H}_{XY} + \mathcal{H}_0$, where $\mathcal{H}_0$ is an anisotropic extra term. By properly choosing the lattice geometry and resonant modes within the cavities, one can obtain the ground state associated with the XY Hamiltonian $\mathcal{H}_{XY}$ emerging as the lasing supermode. Under these circumstances, depending on the mode number n and number of array elements N, various scenarios are expected to arise. For instance, when nanodisks are emitting in a TE_{22} mode ($n = 2$), one can see from Eq. (3) that the equivalent spin exchange interactions are FM, i.e., $J_{ij} < 0$. Figure 3A shows an array of such nanolasers with $N = 4$ elements, together with its lasing supermode, corresponding to the ground state of its XY Hamiltonian counterpart. To further investigate such FM behavior, we extended this same structure to a larger square lattice. Figure 3B illustrates the expected ground state of such an arrangement, signifying all the elements lasing in unison. As mentioned earlier, by utilizing various resonant modes within individual cavity elements in a nanolaser lattice, one would be able to change the way the ensuing pseudospins interact with each other. To demonstrate this, let us assume each nanocavity is now predominantly oscillating in a TM_{21} EM mode. In this scenario, for an array arranged in a square geometry, the Hamiltonian of Eq. (5) represents an XY Hamiltonian with AF exchange interactions $J_{ij} > 0$. This behavior is clearly evident in our FEM simulations presented in Figure 3C. Similar AF states also arise in large square lattices comprising nanodisk lasers emitting in the same TM_{21} mode (Figure 3D).

2.3 Geometric frustration in nanolaser arrays

So far, in all the cases considered in our study, the nanolaser system was able to reach the minimum of the energy landscape function by minimizing the corresponding local energy exchange interactions. We now consider scenarios where the competing interactions between nearby elements tend to prevent the system from reaching a global minimum of the Hamiltonian function. This phenomenon – known as
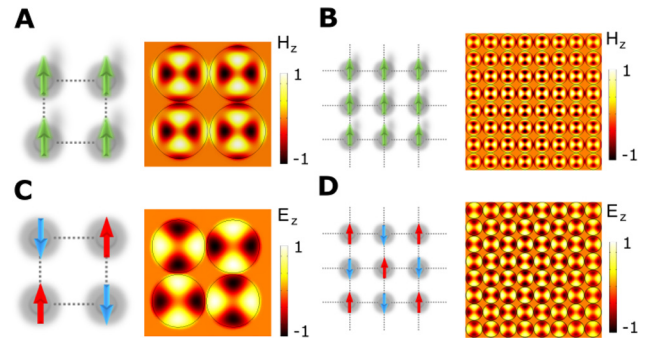

Figure 3: Ferromagnetic and antiferromagnetic XY Hamiltonians in various geometries. (A) A four-element nanodisk laser where a TE_{22} mode is dominantly lasing. The corresponding ground state is obtained from FEM simulations. (B) Square lattice of nanodisk lasers emulating a lattice of FM coupled magnetic spins. (C), (D) Similar geometries for nanodisk cavities lasing in a TM_{21} mode, where an AF exchange interaction is expected to arise between nearby elements.

geometric frustration – results from an incompatibility between a local order which is dictated by the Hamiltonian, and the geometrical constraints present in the system. Such frustrated ground states occur in various arrangements ranging from ice [31] to blue phases in liquid crystals [32]. In order to demonstrate such states in our nanolaser platform, we implement the TE_{1m} family of lasing modes within the nanocavities, hence resulting in positive $J_{ij} > 0$ exchange couplings, associated with AF interactions in the XY Hamiltonian of Eq. (5). We then simulated arrays of such nanolasers with $N = 3$ and $N = 5$ elements. As is well known, the ground state of the XY Hamiltonian with AF exchange interactions in these geometries exhibits geometric frustration, with a 120° and 144° successive rotation between the nearby pseudospins. As depicted in Figure 4A, B, such frustrated ground states are clearly observed in our FEM simulations involving these structures. In magnetic materials, an important example of geometric frustration arises in kagome antiferromagnets [33, 34]. Figure 4C shows a schematic representation of an AF kagome lattice, where a possible ground state has also been depicted. Our simulations confirm that the lasing supermode of a kagome nanolaser array with AF exchange interactions exhibits the same frustrated behavior (Figure 4C).

3 Discussion

In all the cases discussed in our study, the relevant exchange interactions J_{ij} can be adjusted via tuning the metallic gaps between adjacent nanocavities. This changes
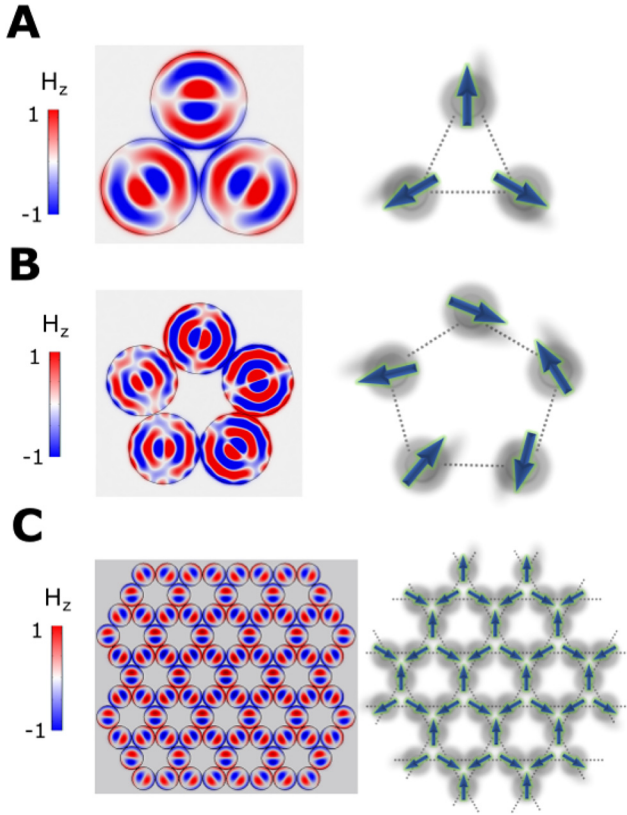
Figure 4: Geometric frustration in the XY Hamiltonian with AF couplings. (A) Lasing in the TE_{13} and (B) TE_{14} resonant modes of nanodisk lasers arranged in arrays of three and five elements, respectively. In these scenarios, the structure emulates an AF exchange interaction among nearest-neighbor elements, where the ground state is expected to show geometric frustration. The FEM simulations indeed confirm such behavior with 120° and 144° successive rotation between consecutive elements in (A) and (B), respectively. (C) Kagome lattice of nanodisk lasers with AF exchange interactions. A frustrated lasing supermode is observed in simulations, as expected from the ground state shown in the right.

the strength of the overlapping near-fields of the nanolasers and therefore enables implementing more general Ising and XY Hamiltonians with unequal exchange couplings. Moreover, the fact that arrays of nanolasers have ultra-small footprints means that in practice one could fabricate many different versions of a spin Hamiltonian with various exchange interactions on a single chip. By simultaneously using the data acquired from all such variations, one could effectively address the issue of reconfigurability in nanolaser lattices intended for Hamiltonian optimization. Another approach that could potentially address the issue of reconfigurability is to partially use gain material in the gap region between the resonators. By proper pumping of this gain material, one can then adjust the coupling strength between the neighboring

elements. In addition, as discussed before, the resulting exchange couplings in arrays of nanolasers are by nature limited to nearest-neighbor interactions. A possible extension to more complicated Hamiltonians where couplings among remote pseudospins are needed can be achieved via introducing auxiliary nanolaser elements that provide effective couplings beyond adjacent elements, similar to quantum computation strategies [35].

4 Conclusion

In conclusion, we showed arrays of active metallic nanocavities can be utilized to emulate spin-Hamiltonians. Such nanoscale structures support vectorial optical resonant modes that exhibit similar behavior as interacting magnetic spins. Depending on the geometry, our analytical expressions for the total electromagnetic losses in the metallic cladding are formally equivalent to various types of spin-exchange Hamiltonians. In particular, we demonstrated Ising and XY Hamiltonians with both ferromagnetic and antiferromagnetic interactions in our platform. In some scenarios, the competing AF interactions among nearby pseudospins resulted in geometric frustration in the associated electromagnetic modes. In all cases, our FEM simulations were in agreement with the theoretically predicted behaviors. It should be emphasized that for all the scenarios considered here, our linear analysis successfully predicts the steady-state behavior of the nanolaser system. However, as the size and connectivity of the implemented spin Hamiltonian increases, it is generally expected that a more complicated energy landscape will emerge. This latter effect, together with higher-order nonlinear phenomena may preclude the system from settling into the ground state corresponding to the linear Hamiltonian. In our future steps, we plan to investigate the nonlinear dynamics associated with such regimes of behavior in our system. Our results pave the way for an ultracompact, on-chip platform for implementing spin Hamiltonians with potential computational benefits.

References

[1] S. Rudich and A. Wigderson, *Computational Complexity Theory*, vol. 10. American Mathematical Society, 2004.

[2] A. M. Turing, "On computable numbers, with an application to the Entscheidungsproblem," *J. Math.*, vol. 58, pp. 345–363, 1936.

[3] V. Iyengar, K. Chakrabarty, and E. J. Marinissen, "Efficient test access mechanism optimization for system-on-chip," *IEEE Trans. Comp. Aid. Des. Integ. Cir. Sys.*, vol. 22, pp. 635–643, 2003.

[4] G. Schneider and U. Fechner, "Computer-based de novo design of drug-like molecules," *Nat. Rev. Drug Dis.*, vol. 4, pp. 649–663, 2005.

[5] S. Fortunato, "Community detection in graphs," *Phys. Rep.*, vol. 486, pp. 75–174, 2010.

[6] G. D. Cuevas and T. S. Cubitt, "Simple universal models capture all classical spin physics," *Science*, vol. 351, pp. 1180–1183, 2016.

[7] S. Kirkpatrick, C. D. Gelatt, and M. P. Vecchi, "Optimization by simulated annealing," *Science*, vol. 220, pp. 671–680, 1983.

[8] Y. Fu and P. W. Anderson, "Application of statistical mechanics to NP-complete problems in combinatorial optimisation," *J. Phys. A.*, vol. 19, p. 1605, 1986.

[9] I. Bloch, J. Dalibard, and S. Nascimbène, "Quantum simulations with ultracold quantum gases," *Nat. Phys.*, vol. 8, pp. 267–276, 2012.

[10] J. Struck, C. Ölschläger, R. Le Targat, et al., "Quantum simulation of frustrated classical magnetism in triangular optical lattices," *Science*, vol. 333, pp. 996–999, 2011.

[11] S. Trotzky, P. Cheinet, S. Fölling, et al., "Time-resolved observation and control of superexchange interactions with ultracold atoms in optical lattices," *Science*, vol. 319, pp. 295–299, 2008.

[12] J. Struck, M. Weinberg, C. Ölschläger, et al., "Engineering Ising-XY spin-models in a triangular lattice using tunable artificial gauge fields," *Nat. Phys.*, vol. 9, pp. 738–743, 2013.

[13] M. P. A. Fisher, P. B. Weichman, G. Grinstein, and D. S. Fisher, "Boson localization and the super8uid-insulator transition," *Phys. Rev. B*, vol. 40, pp. 546–570, 1989.

[14] A. Marandi, Z. Wang, K. Takata, R. L. Byer, and Y. Yamamoto, "Network of time-multiplexed optical parametric oscillators as a coherent Ising machine," *Nat. Photon.*, vol. 8, pp. 937–942, 2014.

[15] P. L. McMahon, A. Marandi, Y. Haribara, et al., "A fully programmable 100-spin coherent Ising machine with all-to-all connections," *Science*, vol. 354, pp. 614–617, 2016.

[16] R. Hamerly, T. Inagaki, P. L. McMahon, et al., "Experimental investigation of performance differences between coherent Ising machines and a quantum annealer," *Sci. Adv.*, vol. 5, 2019, eaau0823.

[17] N. G. Berloff, M. Silva, K. Kalinin, et al., "Realizing the classical XY Hamiltonian in polariton simulators," *Nat. Mater.*, vol. 16, pp. 1120–1126, 2017.

[18] P. G. Lagoudakis and N. G. Berloff, "A polariton graph simulator," *New J Phys.*, vol. 19, p. 125008, 2017.

[19] K. P. Kalinin and N. G. Berloff, "Simulating Ising and n-state planar Potts models and external fields with nonequilibrium condensates," *Phys. Rev. Lett.*, vol. 121, p. 235302, 2018.

[20] M. Nixon, E. Ronen, A. A. Friesem, and N. Davidson, "Observing geometric frustration with thousands of coupled lasers," *Phys. Rev. Lett.*, vol. 110, p. 184102, 2013.

[21] V. Pal, C. Tradonsky, R. Chriki, A. A. Friesem, N. Davidson, "Observing dissipative topological defects with coupled lasers," *Phys. Rev. Lett.*, vol. 119, p. 013902, 2017.

[22] M. Babaeian, D. T. Nguyen, V. Demir, et al., "A single shot coherent Ising machine based on a network of injection-locked multicore fiber lasers," *Nat. Commun.*, vol. 10, pp. 1–11, 2019.

[23] D. Pierangeli, G. Marcucci, and C. Conti. "Large-sclae photonic ising machine by spatial light modulation," *Phys. Rev. Lett.*, vol. 122, p. 213902, 2019.

[24] C. Conti and L. Leuzzi, "Complexity in nonlinear disordered media," *Phys. Rev. B*, vol. 83, pp. 134204–134219, 2011.

[25] M. Parto, W. Hayenga, A. Marandi, D. N. Christodoulides, and M. Khajavikhan, "Realizing spin-Hamiltonians in nanoscale active photonic lattices," *Nat. Mater.*, vol. 963, pp. 1–7, 2020.

[26] M. T. Hill, Y. S. Oei, B. Smallburge, et al., "Lasing in metallic-coated nanocavities," *Nat. Photon.*, vol. 1, pp. 589–594, 2007.

[27] M. P. Nezhad, A. Simic, O. Bondarenko, et al., "Room-temperature subwavelength metallo-dielectric lasers," *Nat. Photon.*, vol. 4, pp. 395–399, 2010.

[28] S. H. Kwon, J. H. Kang, C. Seassal, et al., "Subwavelength plasmonic lasing from a semiconductor nanodisk with silver nanopan cavity," *Nano Lett.*, vol. 10, pp. 3679–3683, 2010.

[29] M. Khajavikhan, A. Simic, M. Katz, et al., "Thresholdless nanoscale coaxial lasers," *Nature*, vol. 482, pp. 204–207, 2012.

[30] W. E. Hayenga, H. G. Garcia, H. Hodaei, et al., "Second-order coherence properties of metallic nanolasers," *Optica*, vol. 3, pp. 1187–1193, 2016.

[31] L. Pauling, "The structure and entropy of ice and of other crystals with some randomness of atomic arrangement," *J. Am. Chem. Soc.*, vol. 57, pp. 2680–2684, 1935.

[32] D. C. Wright and N. D. Mermin, "Crystalline liquids: the blue phases," *Rev. Mod. Phys.*, vol. 61, pp. 385–432, 1989.

[33] R. Moessner and J. T. Chalker, "Low-temperature properties of classical geometrically frustrated antiferromagnets," *Phys. Rev. B*, vol. 58, pp. 12049–12062, 1998.

[34] M. E. Zhitomirsky, "Octupolar ordering of classical kagome antiferromagnets in two and three dimensions," *Phys. Rev. B*, vol. 78, pp. 094423, 2008.

[35] M. A. Nielsen and I. Chuang, *Quantum Computation and Quantum Information*, Cambridge, UK, Cambridge University Press, 2000.